Journal of Magnetism and Magnetic Materials 420 (2016) 225–231

Contents lists available at ScienceDirect

Journal of Magnetism and Magnetic Materials

journal homepage: www.elsevier.com/locate/jmmm

Growth mechanism and magnetism in carbothermal synthesized Fe_3O_4 nanoparticles from solution combustion precursors

Xuanli Wang [a], Mingli Qin [a,*], Zhiqin Cao [a,b], Baorui Jia [a], Yueru Gu [a], Xuanhui Qu [a], Alex A. Volinsky [c]

[a] School of Materials Science and Engineering, University of Science and Technology Beijing, Beijing, 100083 China
[b] School of Materials Science and Engineering, Pan Zhihua University, Pan Zhihua, 617000 China
[c] Department of Mechanical Engineering, University of South Florida, Tampa, 33620 USA

ARTICLE INFO

Article history:
Received 14 February 2016
Received in revised form
23 May 2016
Accepted 14 July 2016
Available online 19 July 2016

Keywords:
Solution combustion synthesis
Carbothermal reduction
Magnetite nanoparticles
Growth mechanism
Magnetic properties

ABSTRACT

Magnetic Fe_3O_4 nanoparticles were prepared by carbothermal reduction using solution combustion synthesis precursors derived from ferric nitrate (oxidizer), glycine (fuel) and glucose (carbon source) mixed solution. In this paper, the growth mechanism and magnetism in Fe_3O_4 nanoparticles were investigated by adjusting the glucose content in precursor and the heat temperature in carbothermal process. The products were analyzed by X-ray diffraction, Field emission scanning electron microscopy, Infrared adsorption method and Vibrating sample magnetometry. The results revealed that the more amount of glucose, the earlier Fe_3O_4 phase generated as temperature increasing. Depending on glucose content and thermal temperature, the average grain size of Fe_3O_4 nanoparticles varied from 19.9 nm to 48 nm and saturation magnetization changed from 21.2 emu/g to 71.77 emu/g, which indicated that the saturation magnetization of Fe_3O_4 nanoparticles fell off as the average grain size decreasing. These results were crucial not only from the application stand-point, but more importantly leaded to a new platform for further studies of high quality magnetic Fe_3O_4 particles at nanoscale.

1. Introduction

Magnetite (Fe_3O_4) with brownish-black and metallic luster, is the most strongly magnetic of all the naturally occurring minerals in nature [1]. It has a cubic inverse spinel structure, consists of a cubic close packed array of oxide ions where all of the Fe^{2+} ions occupy half of the octahedral sites and the Fe^{3+} ions are split evenly across the remaining octahedral sites and tetrahedral sites [2,3]. Magnetite has displayed unique electric and magnetic characters ascribing to electron exchange between Fe^{2+} and Fe^{3+} in the octahedral sites [4]. During the past decades, as the nanostructure exhibited novel physical and chemical properties differing from their bulk counterparts [5], the magnetic Fe_3O_4 nanoparticles have attracted considerable attention due to their compatible magnetic and electrochemical properties [6], such as ferromagnetic [7], superparamagnetic [8], saturation magnetization [9], dielectric properties [10] and biocompatibility [11], which endowed these nanoparticles with potential applications in many fields, including ferrofluids [12], catalysts [13], lithium ion batteries [14], microwave absorption [15], magnetic resonance imaging [16], biosensors [17], etc. It was evident that the electric and magnetic performance can be effectively controlled by the morphology and microstructure [18], which were very sensitive and strongly depended on the synthesis method and experimental conditions.

Up to now, there have been a variety of preparation techniques reported to synthesize the magnetic Fe_3O_4 nanoparticles, including high-energy ball milling method [19], co-precipitation [20], micro-emulsion [21], hydrothermal synthesis [22], sol–gel method [23], reduction of hematite by CO [24] and so on. However, some of these approaches encountered limits, including complicated equipment, long preparation time, multiple processing steps or environmental pollution, which rendered them unsuitable for large-scale production economically, or because of environmental concerns [25]. Carbothermal reduction method (CTR) was widely used in the industry to directly reduce metal oxides, using carbon as the reducing agent [26]. Nevertheless, this method also faced difficulties in demands of homogeneously mixing raw materials for fabricating highly pure products [27]. Thus, there was an urgent requirement to develop a method for preparing high purity and uniform mixture as the precursors of CTR. Solution combustion synthesis (SCS) was a versatile, simple and rapid process, which involved a self-sustained reaction in homogeneous solution of different oxidizers (e.g. metal nitrates) and fuels (e.g. urea,

* Corresponding author.
E-mail address: qinml@mater.ustb.edu.cn (M. Qin).

http://dx.doi.org/10.1016/j.jmmm.2016.07.030
0304-8853/

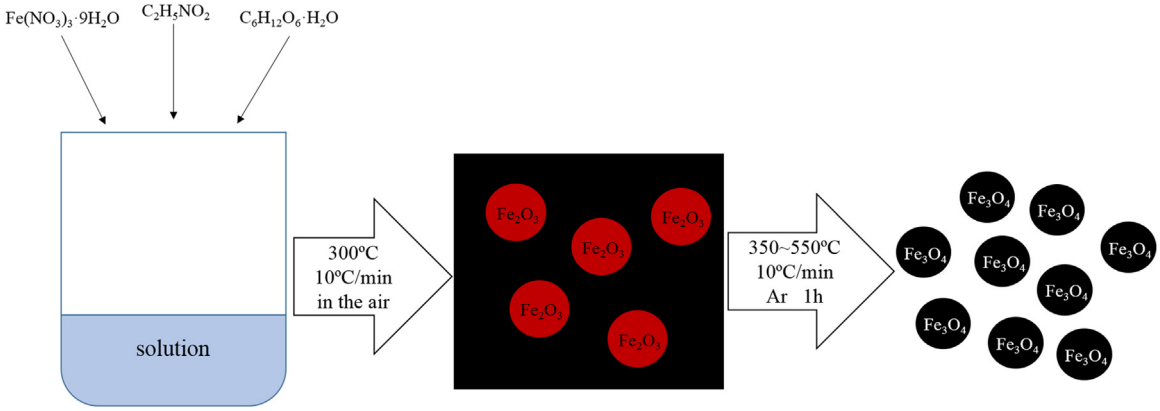

Fig. 1. Schematic illustration of carbothermal synthesis of magnetic Fe_3O_4 nanoparticles from solution combustion precursors.

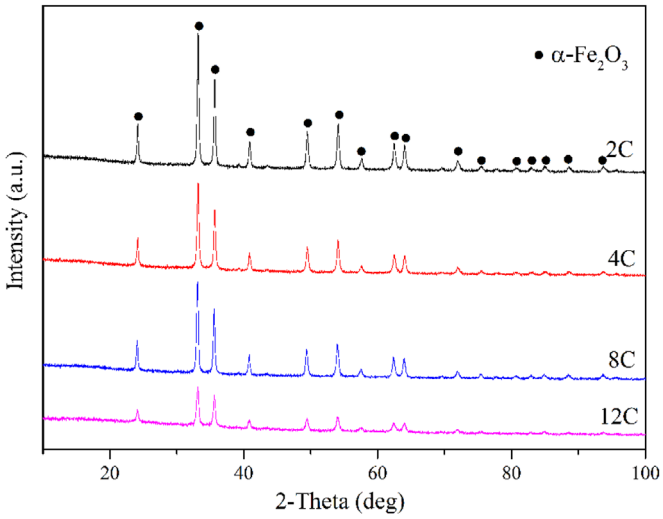

Fig. 2. XRD patterns of precursors obtained by SCS with different glucose contents.

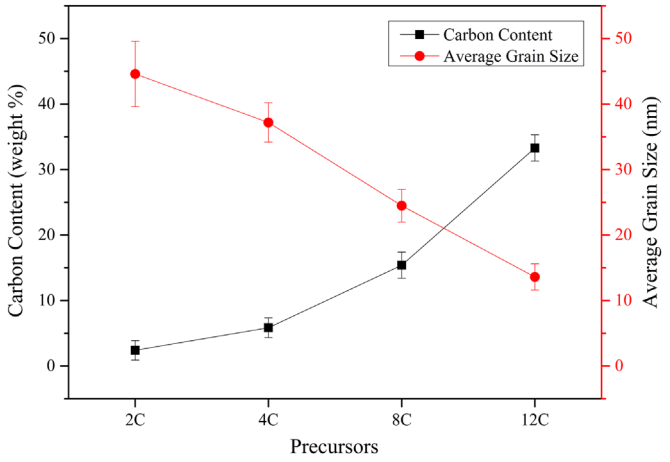

Fig. 3. Carbon content and average grain size of precursors obtained by SCS with different glucose contents.

glycine, hydrazides) [28]. An initial molecular level mixed solution permitted precise and uniform formulation of desired ingredients on the nanoscale. After preheating to a moderate temperature, the mixture self-ignited along the whole volume leading to the formation of fine solid products with tailored composition [29]. The short process duration and the formation of various gases during SCS inhibited particle size growth and favored synthesis of nano-sized powders with high specific surface area [30].

Hence, in this work, we successfully prepared high saturation magnetization Fe_3O_4 nanoparticles by combining SCS with CTR for the first time and provided insight into the growth of magnetic Fe_3O_4 nanoparticles. So far, although a number of researchers have proposed the combination method for the preparation of some oxides, carbides and nitrides [24,26,27], to the best of our knowledge, there was still no literature reporting about the carbothermal synthesis of magnetic Fe_3O_4 nanoparticles by using Fe_2O_3 and amorphous carbon hybrid particles derived from SCS as starting materials. In addition, a possible growth mechanism and magnetic properties of Fe_3O_4 nanoparticles were investigated in detail, so that the high quality magnetic Fe_3O_4 product could be obtained by adjusting the relevant experimental parameters.

2. Materials and methods

2.1. Materials

Ferric nitrate nonahydrate [$Fe(NO_3)_3 \cdot 9H_2O$], glycine($C_2H_5NO_2$) and glucose monohydrate($C_6H_{12}O_6 \cdot H_2O$) were all supplied by Sinopharm Chemical Reagent Co., Ltd., China. All the chemicals were of analytical grade, commercially available and used as received without further purification.

2.2. Precursor preparation

Ferric nitrate nonahydrate (11.8 g), glycine (6.26 g) and glucose monohydrate (2 g, 4 g, 8 g, 12 g, respectively) were dissolved in 150 mL deionized water under stirring to obtain a homogeneous solution. The mixtures were poured into four 2000 mL beakers, and heated up to 300 °C in the air on a temperature-controlled electrical furnace. As heating continued, the solution evaporated and formed a gelatinous mass. In a few minutes, the gel suddenly swelled and accompanied by releasing lots of gases. The whole process of gel swelling and combustion was a self-propagating and non-explosive exothermic reaction, which took short time without any danger of explosion. Finally, the fragile and foamy products consisted of Fe_2O_3 and different contents of carbon were obtained, which named as 2C, 4C, 8C and 12C, respectively, corresponding to the additional mass of glucose.

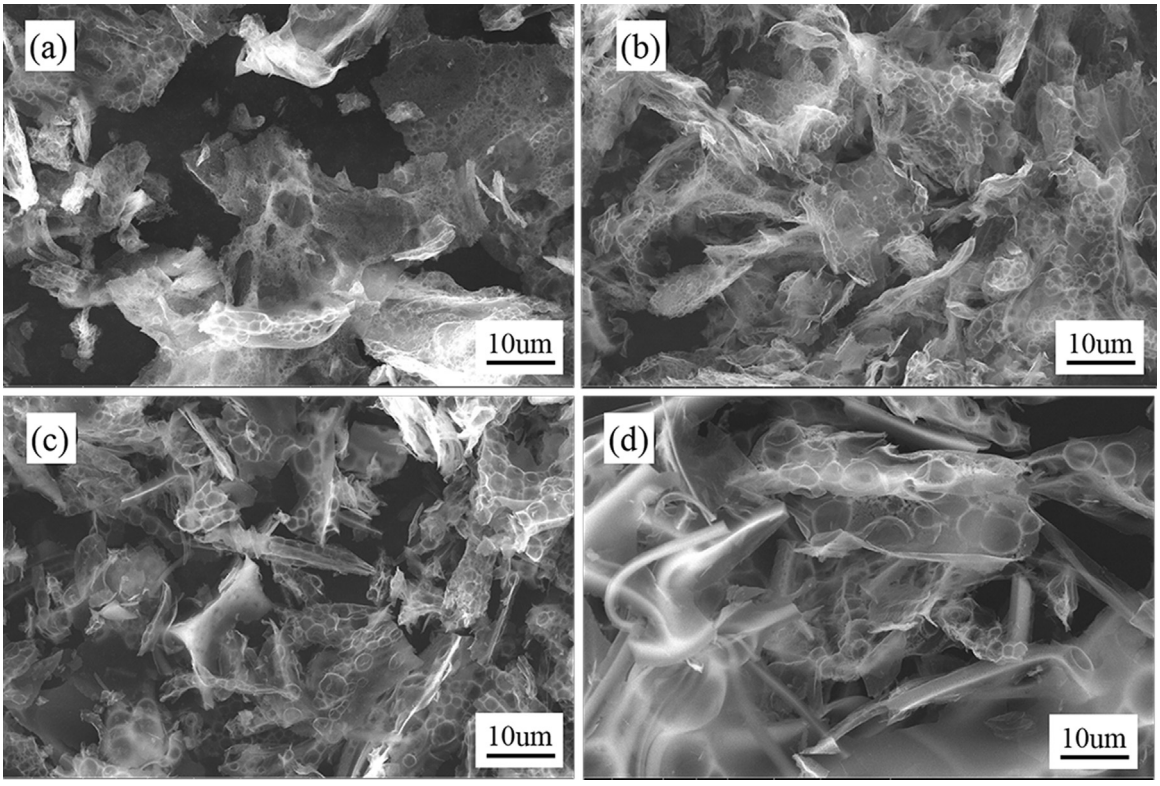

Fig. 4. FE-SEM images of precursors obtained by SCS with different glucose contents: (a) 2 g; (b) 4 g; (c) 8 g; (d) 12 g.

2.3. Thermal treatment

The thermal treatment at different temperatures, 350, 400, 450, 500 and 550 °C, was carried out with 2 g of each sample in argon (150 mL/min) in a quartz tube into a horizontal furnace at a heating rate of 10 °C/min and kept at a final temperature for 1 h. Then, the samples were allowed to cool to room temperature still in the quartz tube under an argon flow for subsequent experiments. The products prepared in this work were named as XC-Y, where $X=2$, 4, 8, 12 corresponding to the amount of glucose in precursors and $Y=350$, 400, 450, 500 or 550 °C.

2.4. Material characterization

Phase analysis of the precursors and calcined products was performed on an X-ray diffractometer (XRD, Ultima IV) equipped with graphite monochromatized Cu Kα radiation as the X-ray source. Data acquisition was performed over the 2θ angular range from 10° to 90° with a scanning speed of 20°/min. The average diameter of crystal was calculated according to the Debye–Scherrer formula [31], $D=K\lambda/\beta\cos\theta$, where D was the crystallite size, K was a constant related to the shape of the crystal, λ was the wavelength of the radiation employed, β was the peak width (full width at half maximum, FWHM) in radians, and θ was the Bragg diffraction angle. Surface morphology of products was observed using field emission scanning electron microscopy (FE-SEM, Quanta FEG-450) at 30 kV. The carbon content was measured by Infrared adsorption method after high frequency induction furnace combustion. Magnetic measurements were carried out using the physical properties measurement system (PPMS) in a vibrating sample magnetometry (VSM, BKT-4500) with a magnetic field up to ±6000 Oe.

3. Results and discussion

Our approach to a novel fabrication process for magnetic Fe_3O_4 nanoparticles principally consisted of solution combustion synthesis and carbothermal reduction method. As illustrated in Fig. 1, this novel process was mainly composed of two steps. The first step involved producing precursors by using ferric nitrate as the oxidizer and using glycine and glucose as fuel and carbon source, respectively. In the synthesis, an aqueous solution of Fe $(NO_3)_3\cdot 9H_2O$, $C_2H_5NO_2$ and $C_6H_{12}O_6\cdot H_2O$ were mixed uniformly, and the resulting mixed solution was heated up to 300 °C at a heating rate of 10 °C/min in the air on a temperature-controlled electrical furnace. As heating continued, the solution evaporated and formed a gelatinous mass. In a few minutes, a gelatinous mass formed and suddenly swelled in subsequent accompanied by releasing lots of gases. Then, the fragile and foamy precursor consisted of Fe_2O_3 and amorphous carbon was obtained. In the second step, the precursor was calcined at a heating rate of 10 °C/min in argon atmosphere at 350-550 °C (at 50 °C intervals) for 1 h to reduce the Fe_2O_3 and thus yielded discrete and homogeneous magnetic Fe_3O_4 nanoparticles.

3.1. Characterization of precursors obtained by solution combustion synthesis

The crystalline structure of precursors, which named herein as 2C, 4C, 8C, 12C, derived from solution combustion synthesis with different contents of glucose were characterized by XRD. As shown in Fig. 2, the patterns could be easily indexed to α-Fe_2O_3 (JCPDS no. 89-8103) [32] according to the diffraction peak positions and relative intensities, which confirmed the hematite structure of these precursors. No additional peaks have been observed indicating that the residual carbon was in amorphous form. Meanwhile, the carbon contents in precursors were presented in Fig. 3. We can see that the amount of glucose in raw materials increased, more

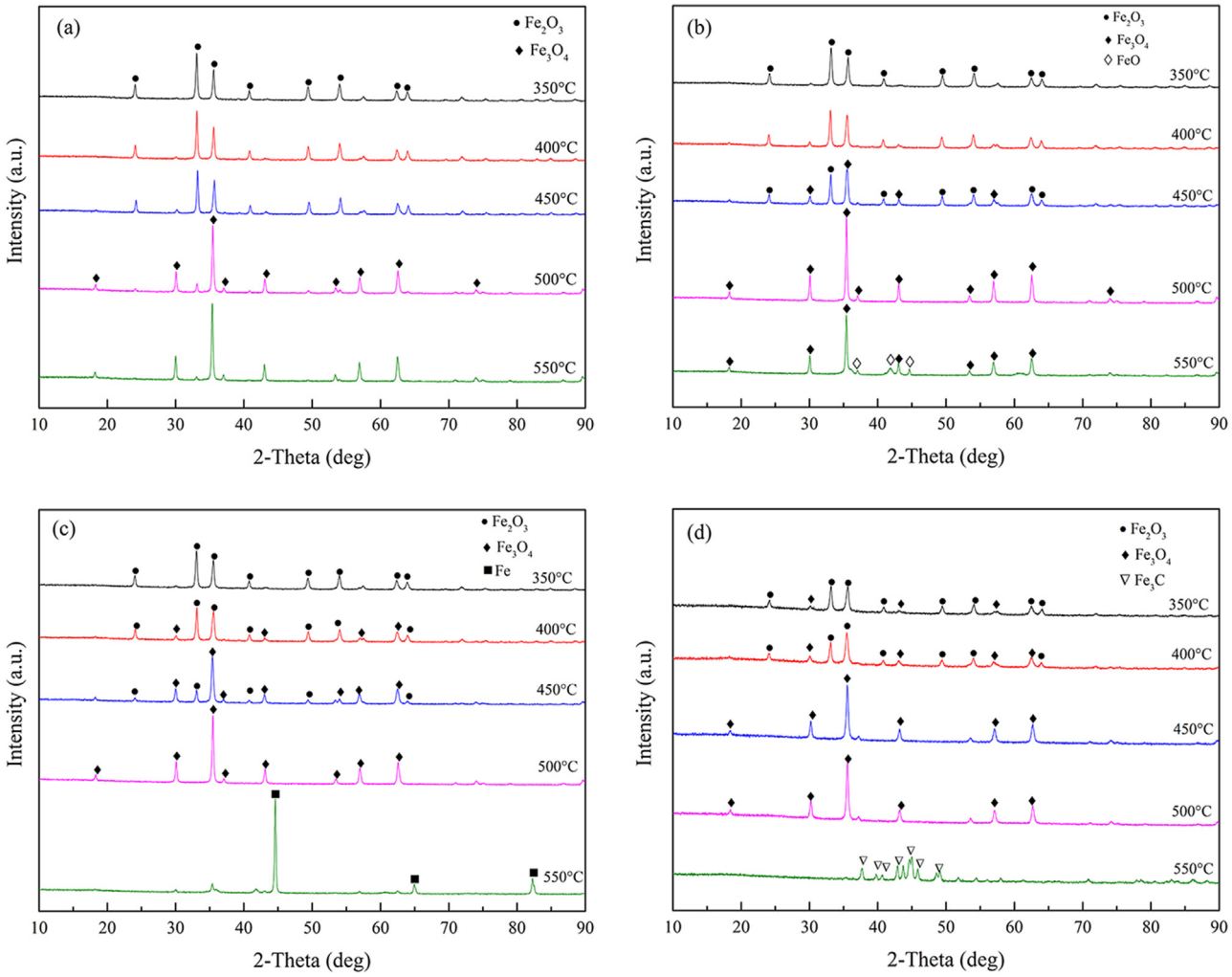

Fig. 5. XRD patterns of thermal treatment products with different temperatures on four precursors: (a) 2C; (b) 4C; (c) 8C; (d) 12C.

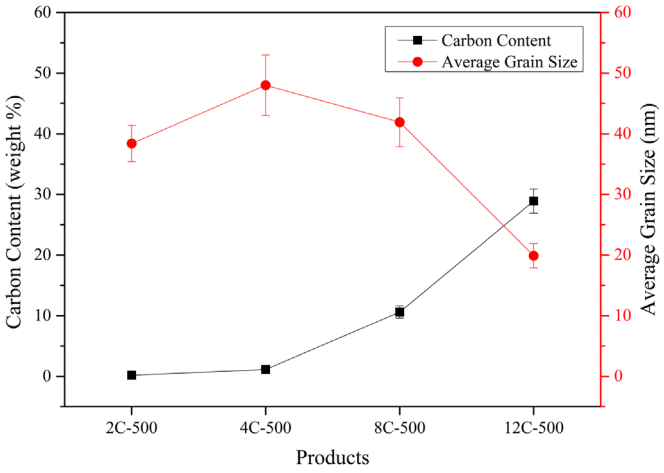

Fig. 6. Carbon content and average grain size of thermal treatment products with different precursors heating at 500 °C.

amorphous carbon were existed in precursor, which corresponding to the less sharp diffraction peaks of α-Fe_2O_3 in Fig. 2. Moreover, it was noticed that the peaks were broader slightly as more glucose added, an indication of the formation of finer particles in nanoscale. The estimated average grain size of the α-Fe_2O_3 nanoparticles deduced from Sherrer's formula were presented in Fig. 3, which were consistent with the tendency obtained from XRD analysis above.

The morphology and microstructure of precursors were investigated by FE-SEM shown in Fig. 4. It can be observed clearly that a significant number of bubbles existed, which were caused by a great many of gases produced in solution combustion process. As temperature elevated, the glucose intermolecular force increased due to the three-dimensional cross-linked structure, thus the viscosity of precursor increased to block gases releasing. Therefore, along with glucose increasing, the size of bubbles grew and the number decreased on account of the increased viscosity and more gases were sealed in the bubbles. It could be also found that the precursors all displayed flaky structure and with glucose content rising, the flake became thinner and larger aspect ration because a large amount of residual carbon hindered grain growth and a great many of gases prevented the agglomeration. According to the above, glucose was not only the reducing agent but also a carbon source, where the quantity of glucose had a great impact on morphology and carbon content of precursor significantly.

3.2. *Fe_3O_4 growth mechanism in carbothermal reduction*

The aforementioned four precursors were treated at 350, 400, 450, 500 and 550 °C for 1 h in Ar atmosphere, respectively. The corresponding products entitled XC-Y, where X represented the amount of glucose in raw mixture, C denoted amorphous carbon and Y stood for the heat treatment temperature.

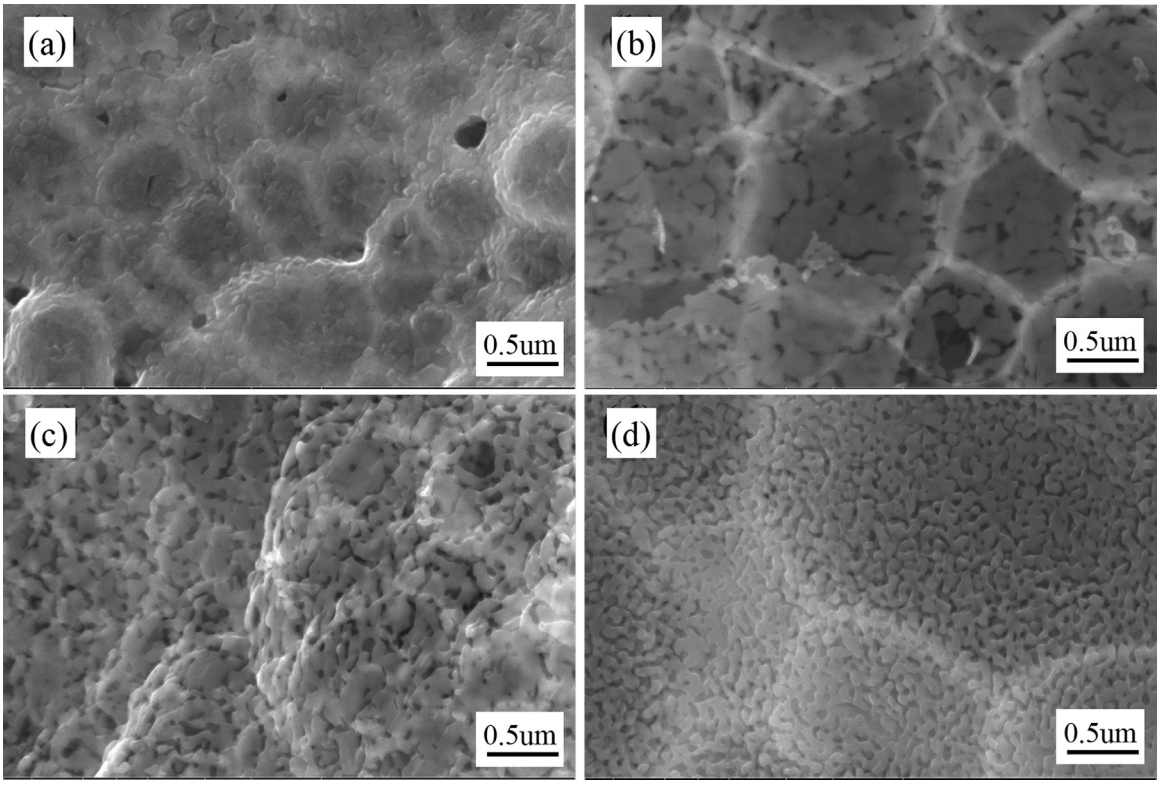

Fig. 7. FE-SEM images of thermal treatment products with different precursors heating at 500 °C: (a) 2C-500; (b) 4C-500; (c) 8C-500; (d) 12C-500.

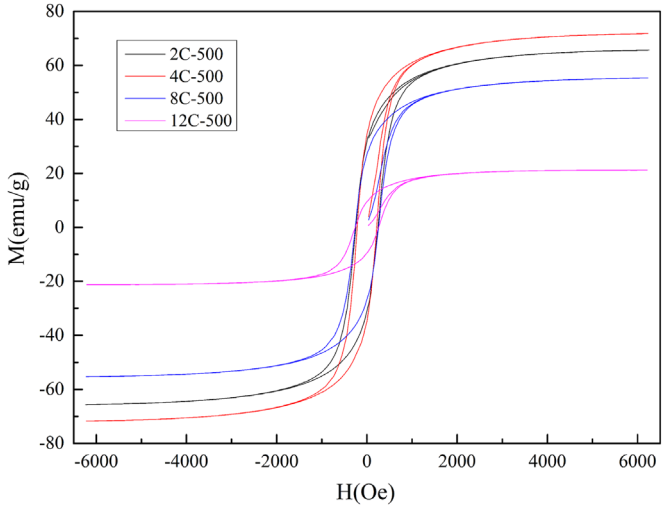

Fig. 8. Room temperature magnetic hysteresis loops of XC-500 products (X=2, 4, 8, 12).

Fig. 5 showed the XRD patterns of thermal treatment products with different heating temperatures on four precursors. As can be seen, 12C precursor began to form Fe_3O_4 since 350 °C, 8C precursor started to become Fe_3O_4 as heated up to 400 °C and 4C precursor changed to Fe_3O_4 when the temperature reached 450 °C. It can be observed that upon the treatment at 500 °C, all the products appeared to transform into Fe_3O_4 (JCPDS no. 65-3107) [32] completely. Since there was no graphite or other characteristic peaks detected in XRD spectrum, the residual carbon contained in these as-synthesized samples were in amorphous state all the same. Moreover, the average grain size of XC-500(X=2, 4, 8, 12) samples estimated by the Scherrer equation and the carbon content of these as-prepared samples were summarized in Fig. 6.

On the one hand, Fig. 5 revealed that when heat treatment temperature raised, Fe_3O_4 phase produced because the nucleation driving force in Fe_2O_3 transformation process enhanced [33]. A new Fe_3O_4 phase formed cores at the interface of grains in Fe_2O_3 parent phase. The higher temperature, the greater driving force and the easier it was to form new cores. Then thermally activation provided atoms adequate energy to jump barriers making the interface migration rate improved. As the cores grew up through interface controlled process, atoms got rid of parent phase across the interface and attached to a new phase [34]. On the other hand, Fig. 5 indicated that the more amount of glucose, the earlier Fe_3O_4 phase generated as a consequence of the reduced nucleation work. That was to say, the increasing amorphous carbon rose the internal crystal defects in grains [35]. In the nucleation process, the cores were inclined to form in these kind of positions, which could slack distortion energy leading to the reduction of nucleation work. Moreover, the crystal defects can also be used as a rapid diffusion channel to accelerate the growth of new Fe_3O_4 phase. Thus, the amorphous carbon derived from glucose pyrolysis could contribute to the formation of a Fe_3O_4 phase at low temperature.

Additionally, in view of the average grain size presented in Fig. 6, we can discover that 4C-500 sample possessed the largest average grain size on account of less carbon content and sufficient reaction from Fe_2O_3 to Fe_3O_4, as shown in Eq. (1). As 2C precursor owned least carbon content, the Fe_3O_4 grain would grow deficiently through Eq. (2), while 8C and 12C owned an excess of carbon, the Fe_3O_4 grain would grow sufficiently through Eq. (1). According to the relationship between carbon content and average grain size presented in Fig. 6, we could find that the average grain size decreased a little before it dropped dramatically to 19.9 nm (even less than 2C-500 sample) as the carbon content increased remarkably, although Fe_2O_3 converted into Fe_3O_4 entirely in XC-500 (X=4, 8, 12) samples. It may be caused by excess carbon content, when the amount of amorphous carbon reached a certain value, it would prevent the grain growth and refined Fe_3O_4 grain [36].

$$3Fe_2O_3+C \rightarrow 2Fe_3O_4+CO \quad (1)$$

$$6Fe_2O_3+C \rightarrow 4Fe_3O_4+CO_2 \quad (2)$$

In addition, FE-SEM micrographs in Fig. 7 confirmed the homogeneous grain size distribution and average grain size trends of XC-500 (X=2, 4, 8, 12) samples, in agreement with the analysis above. Besides, the 2C-500 sample exhibited few large and round pores in Fig. 7(a), while the pores became smaller and narrower along with glucose increasing, as presented in Fig. 7(b)–(d). Since the amount of residual amorphous carbon in precursors enhanced, an increasing number of carbon dioxide or carbon monoxide gases obtained by carbon burning after further heat treatment, the gases would release and improve the porosity in products.

3.3. Magnetism analysis

A measurement of magnetic properties of Fe_3O_4 products XC-500 (X=2, 4, 8, 12) at room temperature were presented in Fig. 8. It can be clearly seen that 4C-500 product had the highest saturation magnetization of 71.77 emu/g while the others were 65.65 emu/g, 55.3 emu/g and 21.2 emu/g corresponding to 2C-500, 8C-500 and 12C-500 product, respectively. Combined with the average grain size results shown in Fig. 6, it was confirmed that the saturation magnetization fell off with grain size decreasing [36]. A detailed analysis of the above relationship was demonstrated below.

In the first place, as Fe_3O_4 grain size reduced, the specific surface area and external phase proportion increased, which would magnify the grain surface defects and led to exterior spin canting, thus the saturation magnetization decreased to some extent. In the second place, Fe_3O_4 had a cubic inverse spinel structure where Fe^{2+} ions and Fe^{3+} ions occupied 4 μB and 5 μB, respectively, which only took spin magnetic moment into account. According to the super-exchange interaction theory, the Fe^{3+} ions located in octahedral and tetrahedral sites possessed opposite spin orientation, thus the net magnetic moment of Fe_3O_4 sprang from the Fe^{2+} ions situated in quarter of octahedral sites randomly. Consequently, when Fe_3O_4 grain size reduced to a certain degree, the magnetocrystalline anisotropy energy was small enough that heat influence surpassed exchange force function, there would be no longer a magnetic moment in fixed easy magnetization direction but the fluctuation in all directions, led to the saturation magnetization decreased in a way. In the third place, with Fe_3O_4 grain size reducing to a single domain state, there was no magnetic domain wall displacement process any more ascribed to none domain walls in granule, thus the low saturation magnetization originated from magnetic domain rotation process exclusively. In addition, the amount of carbon played a key role in saturation magnetization, as the 4C-500 product owned the largest grain size (48 nm) and less carbon content (1.13%), it exhibited the best magnetic performance eventually.

4. Conclusions

In summary, a facile and fast solution combustion synthesis combined with carbothermal reduction method has been demonstrated for the preparation of magnetic Fe_3O_4 nanoparticles. We have obtained magnetite nanoparticles with an average grain size of 48 nm and saturation magnetization of 71.77 emu/g when precursor with 4 g glucose content was heated at 500 °C for 1 h in argon atmosphere. Meanwhile, a possible growth mechanism and magnetic properties of Fe_3O_4 nanoparticles were investigated in detail. The results indicated that the more glucose content, the earlier Fe_3O_4 phase generated and the saturation magnetization of Fe_3O_4 nanoparticles fell off with grain size decreasing and carbon content increasing.

Acknowledgments

This work was financially supported by the National Natural Science Foundation Program of China (51574031, 51574030 and 51574029), the Natural Science Foundation Program of Beijing (2162027), the National 863 Program (2013AA031101), and the Fundamental Research Funds for the Central Universities (06109063).

References

[1] R.J. Harrison, R.E. Dunin-Borkowski, A. Putnis, Direct imaging of nanoscale magnetic interactions in minerals, Proc. Natl. Acad. Sci. USA 99 (2002) 16556–16561.
[2] D. Margulies, F. Parker, M. Rudee, F. Spada, J. Chapman, P. Aitchison, A. Berkowitz, Origin of the anomalous magnetic behavior in single crystal Fe_3O_4 films, Phys. Rev. Lett. 79 (1997) 5162–5165.
[3] C. Yang, J. Wu, Y. Hou, Fe_3O_4 nanostructures: synthesis, growth mechanism, properties and applications, Chem. Commun. 47 (2011) 5130–5141.
[4] S. Si, C. Li, X. Wang, D. Yu, Q. Peng, Y. Li, Magnetic monodisperse Fe_3O_4 nanoparticles, Cryst. Growth Des. 5 (2005) 391–393.
[5] J. Wang, Q. Chen, C. Zeng, B. Hou, Magnetic-field-induced growth of single-crystalline Fe_3O_4 nanowires, Adv. Mater. 16 (2004) 137–140.
[6] Y. Du, W. Liu, R. Qiang, Y. Wang, X. Han, J. Ma, P. Xu, Shell thickness-dependent microwave absorption of core-shell Fe_3O_4@C composites, ACS Appl. Mater. Interfaces 6 (2014) 12997–13006.
[7] B.Y. Geng, J.Z. Ma, X.W. Liu, Q.B. Du, M.G. Kong, L.D. Zhang, Hydrophilic polymer assisted synthesis of room-temperature ferromagnetic Fe[sub3]O [sub4] nanochains, Appl. Phys. Lett. 90 (2007) 043120–043124.
[8] J. Gass, P. Poddar, J. Almand, S. Srinath, H. Srikanth, Superparamagnetic polymer nanocomposites with uniform Fe_3O_4 nanoparticle dispersions, Adv. Funct. Mater. 16 (2006) 71–75.
[9] H. Wang, P. Hu, D. a Pan, J. Tian, S. Zhang, A.A. Volinsky, Carbothermal reduction method for Fe_3O_4 powder synthesis, J. Alloy. Compd. 502 (2010) 1338–1340.
[10] G. Sun, B. Dong, M. Cao, B. Wei, C. Hu, Hierarchical dendrite-like magnetic materials of Fe_3O_4, γ-Fe_2O_3, and Fe with high performance of microwave absorption, Chem. Mater. 23 (2011) 1587–1593.
[11] H. Teymourian, A. Salimi, S. Khezrian, Fe_3O_4 magnetic nanoparticles/reduced graphene oxide nanosheets as a novel electrochemical and bioeletrochemical sensing platform, Biosens. Bioelectron. 49 (2013) 1–8.
[12] M. Klokkenburg, B.H. Erne, J.D. Meeldijk, A. Wiedenmann, A.V. Petukhov, R. P. Dullens, A.P. Philipse, In situ imaging of field-induced hexagonal columns in magnetite ferrofluids, Phys. Rev. Lett. 97 (2006) 185702.
[13] L. Zhou, Y. Shao, J. Liu, Z. Ye, H. Zhang, J. Ma, Y. Jia, W. Gao, Y. Li, Preparation and characterization of magnetic porous carbon microspheres for removal of methylene blue by a heterogeneous Fenton reaction, ACS Appl. Mater. Interfaces 6 (2014) 7275–7285.
[14] J.S. Xu, Y.J. Zhu, Monodisperse Fe_3O_4 and gamma-Fe_2O_3 magnetic mesoporous microspheres as anode materials for lithium-ion batteries, ACS Appl. Mater. Interfaces 4 (2012) 4752–4757.
[15] Z. Wang, L. Wu, J. Zhou, W. Cai, B. Shen, Z. Jiang, Magnetite nanocrystals on multiwalled carbon nanotubes as a synergistic microwave absorber, J. Phys. Chem. C 117 (2013) 5446–5452.
[16] S. Xuan, F. Wang, J.M. Lai, K.W. Sham, Y.X. Wang, S.F. Lee, J.C. Yu, C.H. Cheng, K. C. Leung, Synthesis of biocompatible, mesoporous Fe_3O_4 nano/microspheres with large surface area for magnetic resonance imaging and therapeutic applications, ACS Appl. Mater. Interfaces 3 (2011) 237–244.
[17] M. Shao, F. Ning, J. Zhao, M. Wei, D.G. Evans, X. Duan, Preparation of Fe_3O_4@SiO_2@layered double hydroxide core-shell microspheres for magnetic separation of proteins, J Am. Chem. Soc. 134 (2012) 1071–1077.
[18] J. Ma, K. Wang, M. Zhan, Growth mechanism and electrical and magnetic properties of Ag-Fe_3O_4 core-shell nanowires, ACS Appl. Mater. Interfaces 7 (2015) 16027–16039.
[19] J.F. de Carvalho, S.N. de Medeiros, M.A. Morales, A.L. Dantas, A.S. Carriço, Synthesis of magnetite nanoparticles by high energy ball milling, Appl. Surf. Sci. 275 (2013) 84–87.
[20] J. Baumgartner, A. Dey, P.H. Bomans, C. Le Coadou, P. Fratzl, N.A. Sommerdijk, D. Faivre, Nucleation and growth of magnetite from solution, Nat. Mater. 12 (2013) 310–314.
[21] P.A. Dresco, V.S. Zaitsev, R.J. Gambino, B. Chu, Preparation and properties of magnetite and polymer magnetite nanoparticles, Langmuir 15 (1999) 1945–1951.
[22] T.J. Daou, G. Pourroy, S. Bégin-Colin, J.M. Grenèche, C. Ulhaq-Bouillet, P. Legaré, P. Bernhardt, C. Leuvrey, G. Rogez, Hydrothermal synthesis of monodisperse magnetite nanoparticles, Chem. Mater. 18 (2006) 4399–4404.

[23] Y. Lu, Y. Yin, B.T. Mayers, Y. Xia, Modifying the surface properties of superparamagnetic iron oxide nanoparticles through a sol – gel approach, Nano Lett. 2 (2002) 183–186.
[24] M. Et-Tabirou, B. Dupre, C. Gleitzer, Hematite single crystal reduction into magnetite with CO–CO_2, Metall. Trans. B 19 (1988) 311–317.
[25] P. Hu, S. Zhang, H. Wang, D. a Pan, J. Tian, Z. Tang, A.A. Volinsky, Heat treatment effects on Fe_3O_4 nanoparticles structure and magnetic properties prepared by carbothermal reduction, J. Alloy. Compd. 509 (2011) 2316–2319.
[26] J.P. Murray, A. Steinfeld, E.A. Fletcher, Metals, nitrides, and carbides via solar carbothermal reduction of metal oxides, Energy 20 (1995) 695–704.
[27] H. Wu, M. Qin, A. Chu, Q. Wan, Z. Cao, Y. Liu, X. Qu, A.A. Volinsky, AlN powder synthesis by sodium fluoride-assisted carbothermal combustion, Ceram. Int. 40 (2014) 14447–14452.
[28] S.T. Aruna, A.S. Mukasyan, Combustion synthesis and nanomaterials, Curr. Opin. Solid State Mater. Sci. 12 (2008) 44–50.
[29] K. Deshpande, A. Mukasyan, A. Varma, Direct synthesis of iron oxide nanopowders by the combustion approach: reaction mechanism and properties, Chem. Mater. 16 (2004) 4896–4904.
[30] A.S. Mukasyan, P. Epstein, P. Dinka, Solution combustion synthesis of nanomaterials, Proc. Combust. Inst. 31 (2007) 1789–1795.
[31] U. Holzwarth, N. Gibson, The Scherrer equation versus the 'Debye-Scherrer equation', Nat. Nanotechnol. 6 (2011) 534.
[32] W.M. Zhang, X.L. Wu, J.S. Hu, Y.G. Guo, L.J. Wan, Carbon coated Fe_3O_4 nanospindles as a superior anode material for lithium-ion batteries, Adv. Funct. Mater. 18 (2008) 3941–3946.
[33] M.V. Massa, K. Dalnoki-Veress, Homogeneous crystallization of poly (ethylene oxide) confined to droplets: the dependence of the crystal nucleation rate on length scale and temperature, Phys. Rev. Lett. 92 (2004) 255509.
[34] S. Offerman, N. Van Dijk, J. Sietsma, S. Grigull, E. Lauridsen, L. Margulies, H. Poulsen, M.T. Rekveldt, S. Van der Zwaag, Grain nucleation and growth during phase transformations, Science 298 (2002) 1003–1005.
[35] J. Robertson, "Amorphous carbon", Adv. Phys. 35 (1986) 317–374.
[36] M. George, A. Mary John, S.S. Nair, P.A. Joy, M.R. Anantharaman, Finite size effects on the structural and magnetic properties of sol–gel synthesized $NiFe_2O_4$ powders, J. Magn. Magn. Mater. 302 (2006) 190–195.